Numerical Estimation of Power Deficit and Efficiency in Large Offshore Wind Farms

John M. Prospathopoulos jprosp@cres.gr
George Sieros gsieros@cres.gr
Panagiotis K. Chaviaropoulos tchaviar@cres.gr
Centre of Renewable Energy Sources and Saving

Abstract:

Power deficit and efficiency polar in modeling large offshore wind farms are estimated using the CRES-flowNS RANS solver and the amended GCL engineering model. The comparison with measurements for the Horns Rev and Lillgrund wind farms indicates that predictions significantly overestimate the power deficit when the wind sector is narrow (*±2.5°).* As the size of the sector increases the agreement between predictions and measurements becomes better and for the wide sector of *±15°* it can be considered quite satisfactory, even in the cases of incomplete wind turbine rows. The systematic over-prediction for narrow sectors raises the question if the uncertainty in the measurement of the wind direction produces artificially low power losses in the wake center. The efficiency polar of the wind farms for the whole range of wind directions (*0-360°)* is well estimated using the amended GCL model calibrated with the CRES-flowNS predictions in specific wind directions. Calibration is made in the sense that the proper approach is used for the velocity deficit estimation depending on the wind direction and the wind turbine distance which affect the shadowing between the wind turbines.

Keywords: Power deficit, offshore wind farms, wake modeling, efficiency polar.

1 Introduction

Reliable wake modelling is important for two reasons: First, the accurate estimation of power losses due to wind turbine wakes constitutes a significant part of the overall wind farm economics. Second, there is a growing need for maximizing the exploitation of the available areas in the land (onshore) or the sea (offshore). As a result the turbines must be installed at the closest possible distances which increases the interaction phenomena and affects the performance as well as the lifetime of the downstream turbines: the power output is reduced and the fluctuating loads increase.

Various models have been developed to simulate the wind turbine wakes. These methodologies, initially developed for single wind turbines have been extended to the simulation of wind farms, where a wind turbine may be located in the wakes of the neighbouring turbines. Evaluation of the main wind farm models was carried out in the context of the UpWind project using experimental data from the Danish offshore wind farm Horns Rev [1]. The complexity of the models involved varies: WAsP [2] is a straightforward linear model, whereas WindFarmer [3] uses simplified inviscid flow relationships for the near wake and parabolized momentum equations for the far wake. Furthermore, WAKEFARM [4] solves the parabolized Navier–Stokes equations everywhere and the more advanced models solve the full 3D Navier–Stokes [5,6]. Predictions were compared with measurements for the wind direction of 270^o at various sector widths ($\pm1^o$, $\pm5^o$, $\pm10^o$, $\pm15^o$). The preliminary results indicated that the CFD models over-predict wake losses in the narrow sectors, while the simpler wind farm models tend to under-predict wake losses unless their coefficients are calibrated to match the observations.

In the context of the EERA-DTOC project the aim was to further assess the performance of the existing wind farm models using a range of high quality cases for model simulation. Thus, a number of benchmark cases were defined to investigate complex relationships between wind speed, wind turbine spacing, turbulence and stability offshore and how well the suite of selected models perform. Detailed experimental data sets from the Horns Rev and Lillgrund offshore wind farms were made available from DTU for comparison with the predictions of the models.

In the present paper, the power deficit predictions of the CRES-flowNS [6] RANS solver are evaluated. Furthermore, predictions of the park efficiency for the whole wind rose

are given with the engineering model GCL [7] calibrated with the CFD predictions for certain wind directions.

2 Numerical models

2.1 CRESflow-NS model

CRESflow-NS [6] [6] is an in-house RANS solver using the Wilcox *k-ω* turbulence model for closure and the actuator disk theory for the simulation of the embedded wind turbines. It has been applied to the simulation of single wind turbine wakes, as well as small and large wind farms in flat and complex terrain [8,9]. The momentum equations are numerically integrated introducing a matrix-free pressure correction algorithm which maintains the compatibility of the velocity and pressure field corrections. Discretization is performed with a finite volume technique using a body-fitted coordinate transformation on a structured curvilinear mesh. Convection terns are handled by a second order upwind scheme bounded through a limiter, whereas centred second order schemes are employed for the diffusion terms. Velocity-pressure decoupling is prevented by a linear fourth order dissipation term added into the continuity equation. The *k-ω* turbulence model has been suitably modified for neutral atmospheric conditions [10]:

$$\alpha = 0.3706, \quad \beta = 0.0275, \quad \beta_* = 0.033, \quad \sigma = 0.5, \quad \sigma_* = 0.5 \tag{1}$$

Stratification is considered through an additional production term *f·G* added to each one of the *k* and *ω* transport equations to account for the buoyancy effect [3] The production term *G* is given from the following relationship [11]:

$$G = -\mu_t \left(\frac{\partial U}{\partial z} \right)^2 \cdot \frac{Ri}{f_m}, \tag{2}$$

where where μ_t is the eddy viscosity and the Richardson number, *Ri*, is estimated as:

$$Ri = \zeta \frac{0.74 + 4.7\zeta}{(1 + 4.7\zeta)^2} \tag{3}$$

and $f_m = 1 + 5\zeta$, with $\zeta = z / L$. The Monin-Obukhov length, *L*, characterizes the stability. The *f* function is estimated for the *k* and *ω* equations (f_k and f_ω) respectively, so that the simplified momentum and transport equations for constant pressure (*dp/dx=0*) are fulfilled. After a proper mathematical analysis, the following functions f_k and f_ω are derived for the *k* and *ω* transport equations:

$$f_k = 1 + 4.9\zeta, \quad f_\omega = -14 \cdot (1 + 1.28\zeta) \tag{4}$$

$$f_k = 1 - 1 / Ri, \quad f_\omega = \frac{1 / Ri - 1}{\sigma \cdot \beta^* \cdot \kappa^2 / \beta^{1.5} - 1} \tag{5}$$

for stable and unstable conditions respectively.

Wind turbine simulation: According to the actuator disk approach, the rotor of each wind turbine is simulated as a disk discretized by a number of control volumes. Each control volume acts as a momentum sink through the actuator force calculated using the following relationship

$$F = 0.5 \rho \, U_{ref}^2 \, C_T \, \Delta S \tag{6}$$

where ρ stands for the air density, U_{ref} is the reference wind speed for the thrust coefficient calculation, C_T is the thrust coefficient and ΔS is the surface area of the control volume.

The reference velocity U_{ref} is estimated at the position of each wind turbine as if the specific turbine was absent. In offshore wind farms, wind turbines are mostly installed in parallel rows, so turbine rows can be considered instead of single turbines. A parabolic procedure activating successively the wind turbine rows is applied: The run starts ignoring the presence of the turbines to estimate the reference velocities at the positions of the first row. When a certain convergence criterion is fulfilled for the velocities at those positions, the actuator disks are activated at the first row. The simulation continues and the reference velocities are estimated at the second row. This procedure is repeated until all turbine rows are added.

Computational domain and boundary conditions: The wind farm is enclosed in a computational domain with assumed known inflow conditions, corresponding to the downstream conditions of the affecting upstream installations. If there is no upstream installation free stream logarithmic profiles for neutral or stratified conditions are applied to the inlet boundary according to the similarity theory [12]. The outflow and the side boundaries are positioned sufficiently far so that Neumann conditions can be applied for the velocities and the *k,ω* turbulence quantities. The inlet and outlet boundaries are positioned *10 D* and *30 D* upstream and downstream of the first and last wind turbine rows respectively. The side boundaries are positioned *10 D* away of the closest wind turbine and finally the top

boundary is positioned nearly *30 D* above sea level. Logarithmic wall functions are implemented for the first grid point above the sea level.

The mesh is kept fine close to the wind turbine rotors in the horizontal *x, y* directions with a minimum grid spacing close to *0.1 D*. Between the turbine rotors successive coarsening and refinement of the grid lines occurs using geometrical progression. In the vertical direction the mesh is constructed fine close to the sea level with the first grid line at a distance of about *0.007 D*. A fine mesh is also constructed in the area of each W/T rotor disk, using *15* grid points along the rotor diameter.

2.2 GCL model

The GCL model [7] encompasses a semi–analytical description of the wake deficit and a set of simple empirical relations providing the relevant characteristics for the turbulence field in the wake. The empirical expressions are based on full scale measurements and are applicable for both stall, pitch and variable speed regulated turbines. One of the boundary conditions for the deficit model has been modified in order to reflect the blocking effect from the ground.

Mean wind deficit: Neglecting the blocking effect originating from the ground, the wake behind a wind turbine is considered as a free turbulence region. The model is based on the presumptions that the wake region can be adequately described by Prandtl's axisymmetric turbulent boundary layer equations [13] [13] and that self-similarity of the profiles holds. Therefore, wake radius δ and centerline velocity U_s follow the power laws of *1/3* and *(-2/3)* respectively. The accurate expressions are obtained using the empirical condition that the radius of the wake at *9.5* rotor diameters is given by

$$R_{9.5} = \frac{1}{2}\left(R_{nb} + min\left(z_{hub}, R_{nb}\right)\right), \qquad R_{nb} = max\left\{1.08D, 1.08D + 21.7\left(I_a - 0.05\right)\right\} \tag{7}$$

where z_{hub} is the hub height, D is the rotor diameter and I_a is the ambient turbulence intensity. This relationship denotes that the expansion of the wake is dominated by ambient turbulence and ensures a minimum turbulence level of 5%. The blocking effect is taken into account by applying a wake radius equal to the mean of z_{hub} and R_{nb} at *9.5D* distance when wake radius exceeds hub height. Thus, the formula for the wake radius becomes:

$$\frac{\delta(x)}{D} = 0.5 \cdot \left(1 + \frac{C_T \cdot x}{x_0}\right)^{1/3}, \qquad x_0 = \frac{9.5 \cdot D}{\left(2 \cdot R_{9.5} / D\right)^3 - 1} \tag{8}$$

where C_T is the thrust coefficient.

The centerline velocity is derived from the momentum integral in the wake region:

$$\frac{U_s(x)}{U_\infty} = \frac{35}{72} \cdot \left(\frac{D}{\delta(x)}\right)^2 \cdot C_T \tag{9}$$

where U_∞ is the ambient wind speed.

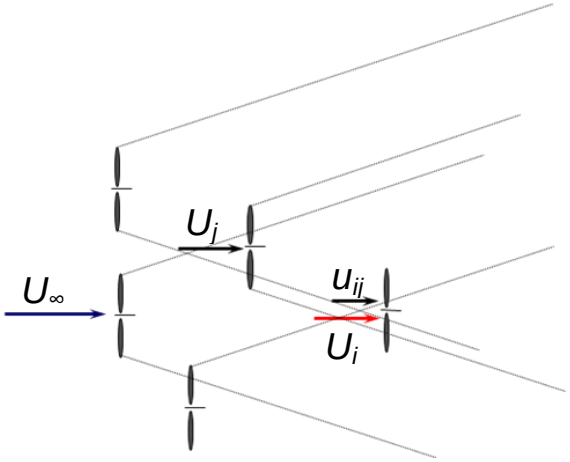

Figure 1: Schematic representation of the interaction between the *i-th* and *j-th* wind turbines. U_j, U_j are the onset velocities of the *i-th*, *j-th* wind turbines and u_{ij} is the velocity induced to the *i-th* wind turbine by the wake of the *j-th* wind turbine

Application to wind farms: GCL model was developed for the estimation of the velocity deficit and the turbulence level within the wake of a single wind turbine. In the case of a wind farm, a wind turbine is subject to the effect of multiple wakes. To calculate the incoming speed on the rotor of the *i-th* wind turbine, the individual effects are summed up according to:

$$\left(U_\infty - U_i\right)^2 = \sum_{j=1}^{N_T}\left[\left(U_j - u_{ij}\right)^2\right] \tag{10}$$

where U_j, U_j are the onset velocities of the *i-th*, *j-th* wind turbines respectively and u_{ij} is the velocity induced to the *i-th* wind turbine by the

wake of the *j-th* wind turbine, estimated through Eq.(8), as shown schematically in Figure 1.

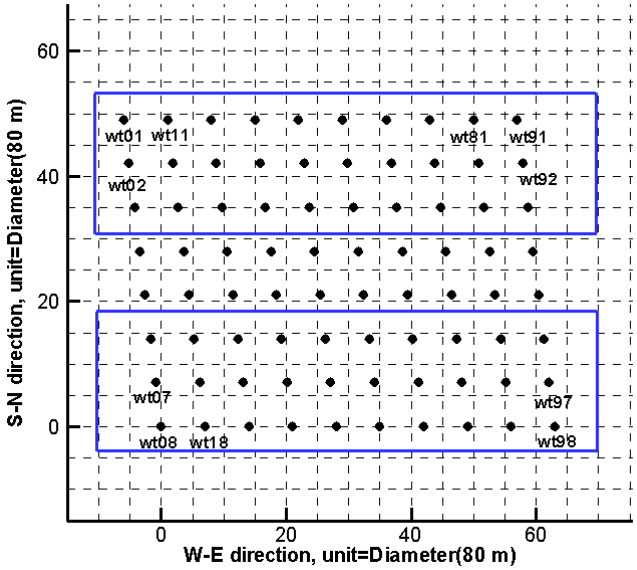

Figure 2: Layout of the Horns Rev offshore wind farm [14]

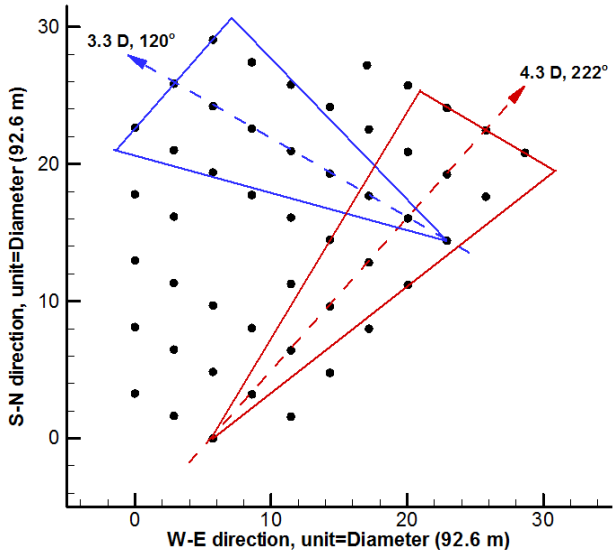

Figure 3: Layout of the Lillgrund offshore wind farm [15]. The *30°* inflow sectors along complete rows of wind turbines are marked for the 120° and 222° wind directions

3 Simulation of test cases

3.1 Description of the wind farms

Horns Rev wind farm: The Horns Rev wind farm has a rated capacity of *160 MW* comprising 80 wind turbines with *80 m* diameter and *70 m* hub height, arranged in a regular array of *8* by *10*, with a spacing of *560 m* in both directions. The layout of the wind farm, shown in Figure 2, is not completely rectangular, while the direction of the N-S columns is *353°*. The wind turbines are installed with an internal spacing along the main directions of *7 D*. The diagonal wind turbine spacing is either *9.4 D* or *10.4 D*. The wind has been in operation since 2004 and the SCADA statistics from 2005-2007 is available for the wake analysis [14]**.**

Lillgrund wind farm: The Lillgrund wind farm comprises 48 wind turbines of *92.5m*

diameter and *65m* hub height, arranged in 8 SW-NE rows (Figure 3). The internal spacing along the directions *222°* and *120°* is *4.3D* and *3.3D*, respectively. The layout is dominated by the triangular shape and two "missing" turbines inside the wind farm.

3.2 Numerical simulation

Horns Rev wind farm: In order to simulate the western wind directions *(270^o±15^o)*, *12* sub-sectors of *2.5^o* were considered. For each one of the sub-sectors the mean wind direction was simulated, e.g. for the sub-sector *270^o-2.5^o*, the simulated mean wind direction was *268.75^o*. Next, two sub-domains, marked with blue lines in Figure 2, were considered. The first one including rows *1-3* was used for the simulation of the wind directions *268.75^o-283.75^o* and the second one including rows *6-8* was used for the simulation of the wind directions *256.25^o - 266.25^o*. It was found that when the first sub-domain was used, rows *1-3* were not affected by the wind turbine wakes from rows *4-8*. In addition, the flow field at the *4^{th}-8^{th}* rows was similar to the flow field at the *3^{rd}* row. In the same way, when the second sub-domain was used, rows *6-8* were not affected by the wind turbine wakes from rows *1-5* and the field at the *1^{st}-5^{th}* rows was similar to the flow field at the *6^{th}* row. Thus, simulation of one sub-domain instead of the whole wind farm is acceptable and saves significant computational cost.

For each simulation, the x-axis of the computational domain was aligned to the wind direction resulting in a transformation of the coordinates of the W/T positions. A successive refinement and coarsening of the grid lines was made in order to achieve a fine mesh close to the W/T positions. The minimum grid size in both *x* and *y* directions was between *0.1 D* and *0.15 D*

Estimation of the reference velocities at the wind turbine positions, required for the thrust and power calculation is performed using the parabolic procedure described in Section 2.1. The convergence of the momentum equations for the *273.75^o* wind direction is shown in Figure 4. The appearance of peaks indicates the activation of each wind turbine column

Lillgrund wind farm: The *222±15°* and *120±15°* wind direction sectors were simulated. A procedure similar to that of the Horns Rev wind farm case was followed, considering 12 sub-sectors of *2.5^o* for each one of the wind sectors and simulating the mean wind direction. However, in this case, all 48 wind turbines were included in each computational run, since there is no repetitive pattern as in the Horns Rev wind farm.

A successive refinement and coarsening of the grid lines was made in order to achieve a fine mesh close to the wind turbine positions. The minimum grid size in both *x* and *y* directions was between *0.08 D* and *0.125 D.* Again, the parabolic activation of wind turbine rows was used for the estimation of reference velocity U_{ref} at the turbine positions

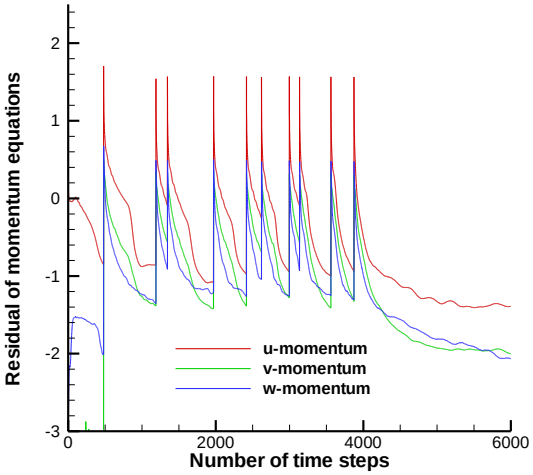

Figure 4: Convergence of the momentum equations for the *273.75^o* wind direction. The appearance of peaks indicates the activation of each wind turbine column

4 Results

4.1 Power deficit

In the Horns Rev test case the inflow mean velocity at hub height (*70 m*) was *8 m/s* and the inflow turbulence intensity at hub height was *7%*. Three cases were defined to validate the influence of the flow sector size for western wind directions: *270^o±2.5^o*, *270^o±7.5^o* and *270^o±15^o*. Numerical simulations were performed with a step of *±2.5^o* starting from *270^o±1.25^o*. In order to estimate the power output for the flow sector *270^o±2.5^o*, the average of the *270^o+1.25^o* (middle of the *270^o+2.5^o* sector) and *270^o-1.25^o* (middle of the *270^o-2.5^o* sector) simulations was calculated. Accordingly, to estimate the power output for the flow sector *270^o±7.5^o*, the average of the *270^o±1.25^o*, *270^o±3.75^o* and *270^o±6.25^o* simulations was calculated.

The power deficit is determined with respect to the reference turbine wt07. The mean power deficit is determined by averaging the results for rows *2-7* as function of spacing. The

predicted mean power deficits are compared with measurements in Figure 5. It is observed that the agreement between predictions and measurements is improved as the flow sector size increases. For a size of *±15°* predictions well agree with the measurements.

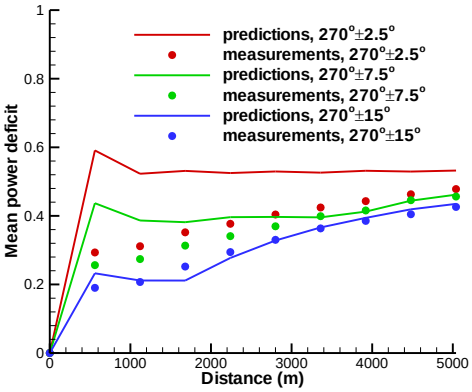

Figure 5: Horns Rev - Mean power deficit along the rows *2* to *7*, obtained by averaging the power output from wind turbines wt02 to wt97 within each row. Predictions and measurements are plotted for three different flow sectors around the *270°* wind direction. The level of turbulence intensity is *7%*.

In the Lillgrund test case, the inflow mean velocity at hub height (*65 m*) was *9 m/s* and the inflow turbulence intensity at hub height was *6%*. *2x7* principal cases were defined to evaluate the influence of the flow sector. The first set of *7* cases referred to the *120±15°* sector, each case corresponding to a *2.5°* sub-sector around a mean wind direction varying from *105°* to *135°*. The power deficit was estimated along a single row of 8 turbines, with an internal spacing of *3.3D*. The second set of *7* cases referred to the *222±15°* sector, each case corresponding to a *2.5°* sub-sector around a mean wind direction varying from *207°* to *232°*. The power deficit was estimated along a single row of 8 turbines, with an internal spacing of *4.3 D*

The predicted power variations along the complete wind turbine rows marked in Figure 3 for the *120±15°* wind sector (*3.3 D* internal spacing) and the *222±15°* wind sector (*4.3 D* internal spacing) are shown in Figures 6,7 when averaging is performed for each one of the *2.5°* sub-sectors. CFD predictions over the *2.5°* sub-sectors show a larger variation of the power deficit in comparison to the measurements, as the wind direction changes from *105°*to *120°* (Figure 6). Both predictions and measurements present a nearly symmetrical behaviour around the *120°* direction, justified by the arrangement of the neighbouring wind turbines. Similar observations can be made for the *222±15°* wind sector (Figure 7). Again, there is a larger variation of the predicted power deficit around the central wind direction of *222°* in comparison to the measurements, especially at the front wind turbines. When averaging is performed over the wider sector of *±15°,* the agreement between predictions and measurements is quite satisfactory (Figure 8), which is similar to what was found in the Horns Rev wind farm case.

Power is also predicted along the incomplete wind turbine rows marked in Figure 9 for the *120±15°* and the *222±15°* wind sectors. CFD predictions over the *2.5°* sub-sectors present again a larger variation of the power deficit in comparison to the measurements. The averaged predicted values over the *±15°* sector agree well with the measurements as shown in Figure 10. As expected, the effect of the 2 missing wind turbines (*3.3 D* internal spacing) is the significant power increase of the turbine which is located *9.9 D* behind its neighbouring upstream machine. Measurements indicate a 86.2% power increase in comparison to the complete wind turbine case, whereas predictions show a 80.6% increase. In the case of 1 missing wind turbine (*4.3 D* internal spacing), the effect of the absent wind turbine is a power increase of almost 35% in its downstream turbine.

4.2 Efficiency polar

The power efficiency for *0 - 360°* inflow was estimated using the amended GCL engineering model [7], calibrated with the CRES-flowNS predictions for specific wind directions. Power efficiency is defined as the ratio between the park power and the power from N_{tot} stand-alone wind turbines where N_{tot} is the total number of turbines.

For the Horns Rev case the wind directions of *270°, 221°* and *312°* were simulated by CRES-flowNS in order to calibrate the engineering model. For each wind direction *α,* the results of 5 simulations performed in the sector *α±2.5°,* with a step of *2.5°*, were averaged to be comparable to the CFD results. According to the standard procedure, the velocity deficit at each wind turbine of the farm is estimated by summing up the inductions of the neighbouring turbines using Equation (10). An alternative formulation is to use maximum value of the velocity deficits at each position instead of the Euclidean norm summation

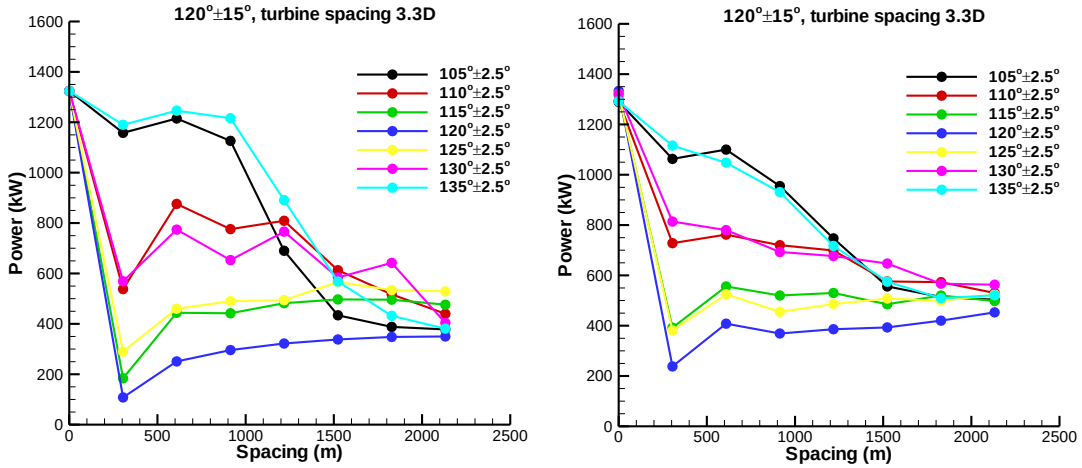

Figure 6: Lillgrund - Power variation along the complete wind turbine rows of Figure 3 for the ±*2.5*^{o} wind sub-sectors around the *120*^{o} wind direction (*30*^{o} wind sector, *3.3 D* internal turbine spacing) (a) Predictions and (b) Measurements

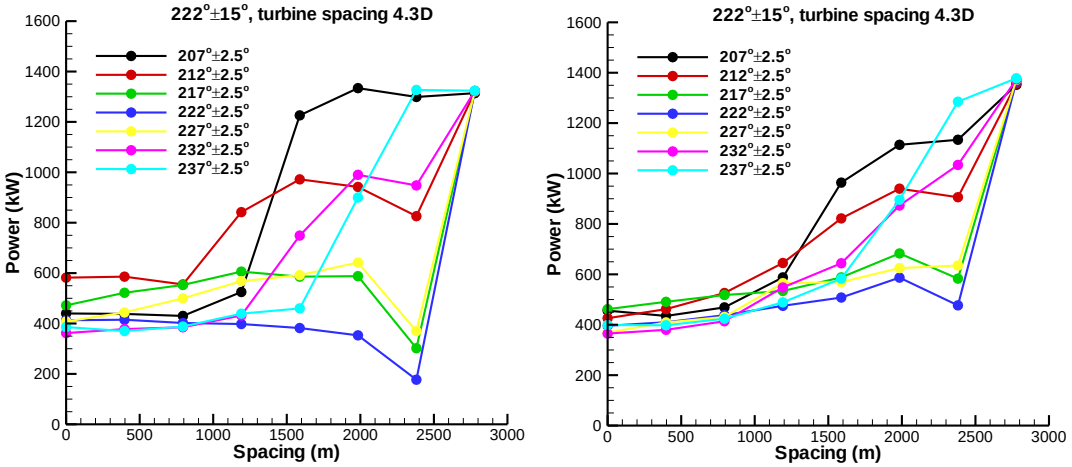

Figure 7: Lillgrund - Power variation along the complete wind turbine rows of Figure 3 for the ±*2.5*^{o} sub-sectors around the *222*^{o} wind direction (*30*^{o} wind sector, *4.3 D* internal turbine spacing (a) Predictions and (b) Measurements

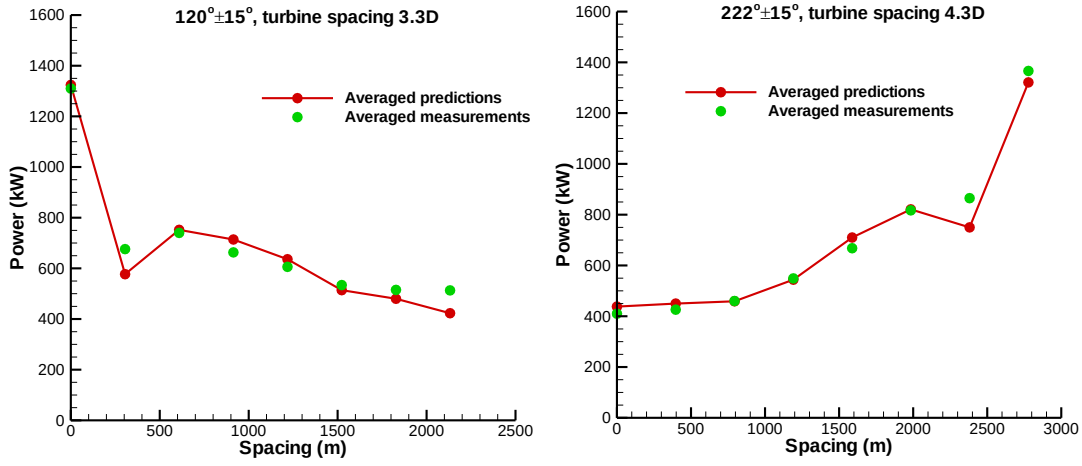

Figure 8: Lillgrund - Average power variation along the complete wind turbine rows of Figure 3. (a) *120*^{o}*±15*^{o} sector with *3.3 D* internal turbine spacing (b) *222*^{o}*±15*^{o} sector with *4.3 D* internal turbine spacing

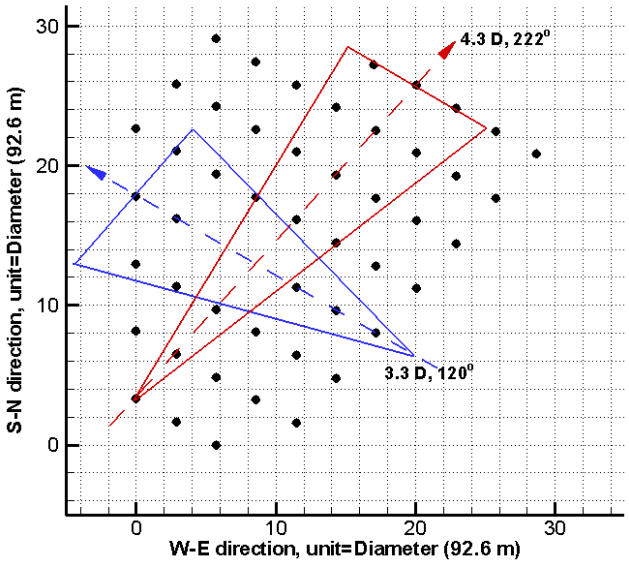

Figure 9: Lillgrund wind farm [15]: *30°* inflow sectors along rows with missing wind turbines are marked for the 120° and 222° wind directions

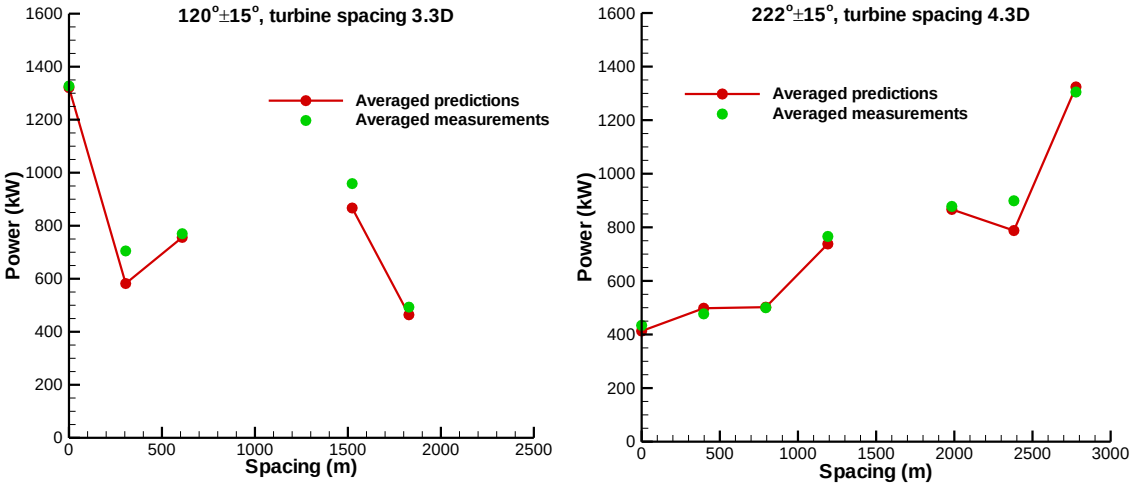

(a) (b)

Figure 10: Lillgrund - Average power variation along the incomplete wind turbine rows of Figure 9. (a) *120°±15°* sector with 2 missing wind turbines (b) *222°±15°* sector with 1 missing wind turbine

The comparison showed that the results of the engineering model are closer to the CFD predictions for all three simulated wind directions when the approach of he maximum velocity deficit is used. However, the overall representation of the wind farm is worse, as seen in Figure 11, where the predictions are compared with the measurements. Due to the nature of the algebraic model used it is seen that there is a concentrated drop in performance around *90°, 180°, 270°, 360°*, which is spread over a larger region in the CFD calculation. The simple approach of adopting the maximum velocity deficit seems to perform better in those wind directions, where the maximum shadowing between the wind turbines occur, but worst in the rest of wind directions. Therefore, a combined method can be adopted to calibrate the engineering model: the maximum velocity deficit approach is used for wind direction sectors centred to multiples of *45°* (works better for multiples of *90°*), whereas the Euclidean norm approach is used for the rest of wind directions. Comparison of the calibrated GCL predictions with measurements is shown in Figure 12. The size of the sectors where the maximum velocity deficit approach is implemented has been selected equal to *7.5°*, however, further investigation is needed to check if this choice is suitable for other wind farms also.

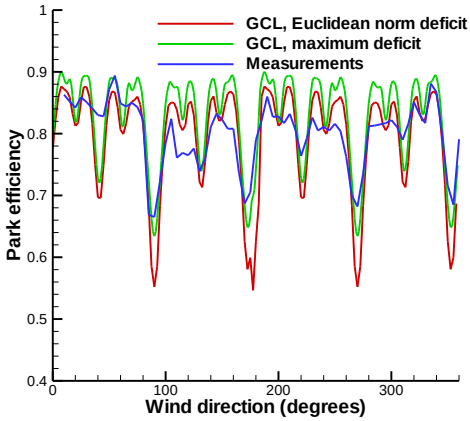

Figure 11: Horns Rev - GCL polar predictions of park efficiency using two different

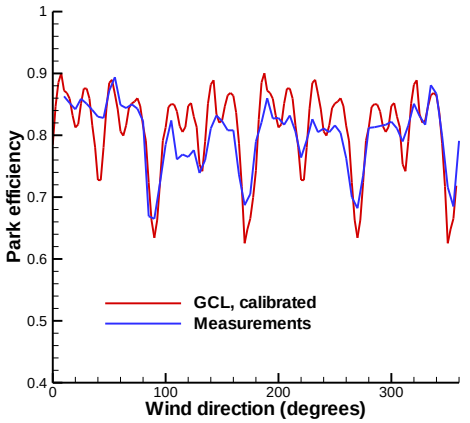

Figure 12: Horns Rev - GCL polar predictions of park efficiency using the calibrated GCL model. The maximum velocity deficit approach is used when the maximum shadowing effect occurs, i.e, when wind direction is a multiple of 45^o.

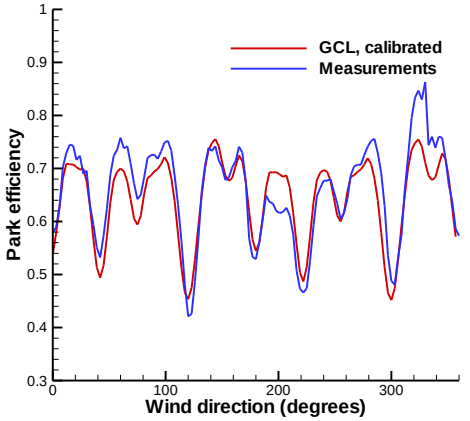

Figure 13: Lillgrund - GCL polar predictions of park efficiency using the calibrated GCL model. The maximum velocity deficit approach is used at all wind directions.

In the Lillgrund wind farm, the distances between the wind turbines are much smaller in comparison to the Horns Rev wind farm resulting in a higher degree of shadowing. As a consequence, the comparison with the CFD predictions shows that the maximum velocity deficit approach of the GCL model performs better than the Euclidean norm approach at all wind directions and not only at the 221° and 120° directions of maximum shadowing. The comparison of the GCL predictions using the maximum velocity deficit approach with measurements is shown in Figure 13

5 Conclusions

The performance of the CRES-flowNS CFD model in large offshore wind farms was evaluated using experimental datasets from the Horns Rev and the Lillgrund wind farms. The comparisons indicated that predictions significantly overestimate the power deficit when the wind sector is narrow (±2.5°). As the size of the sector increases the agreement between predictions and measurements becomes better and for the wide sectors of ±15° it can be considered quite satisfactory.

There is a possibility that part of these large differences is attributed to the uncertainty in the measurement of the wind direction. It should be further investigated if such an uncertainty produces artificially low power losses in the wake centre because of direction variability. Both predictions and measurements predict a high power increase in the cases of incomplete wind turbine rows, but only for the single wind turbine which is located in a larger spacing due to the absence of the missing turbines. The increase in power is more than doubled in the case of two missing turbines in comparison to that of one missing turbine.

The estimation of the wind farm efficiency for the whole wind rose was performed using the amended GCL model calibrated with the CRES-flowNS predictions. In the Horns Rev wind farm the distance between the turbines is 7, 9.4 or 10.4 diameters depending on the wind direction. The comparison with CFD predictions and measurements showed that the maximum velocity deficit approach should be adopted when the ambient flow is aligned with the turbine rows and the maximum shadowing between the wind turbines occurs, whereas the Euclidean norm summation of velocity deficits should be adopted for the rest of wind directions. In the Lillgrund wind farm the distance between the turbines is 4.3 or 3.3 diameters depending on the wind direction. The higher shadowing resulting from the smaller distances between the wind turbines, suggests the usage of the maximum velocity deficit approach for all wind directions. It should be investigated if the wind turbine distance can be

inserted as a parameter to the GCL model, in order to determine the choice of the proper approach at each wind direction. However, simulations in more wind farms are necessary in order to evaluate the effect of the wind turbine distance on the predictions provided by the two different approaches of the GCL model

In general, the comparison with measurements was satisfactory and encouraged the prospect that the combination of fast engineering models with advanced CFD solvers can be used for the prediction of efficiency polar, reducing significantly the computational cost

Acknowledgment

This work was partially funded from the EERA-DTOC project under the context of the 7th Framework Programme (Energy).

References

[1] Barthelmie, R.J., Hansen, K, Frandsen, S.T., Rathmann, O., Schepers, J.G., Schlez, W., Phillips, J., Rados, K., Zervos, A., Politis, E.S., and Chaviaropoulos, P.K., "Modelling and Measuring Flow and Wind Turbine Wakes in Large Wind Farms Offshore", *Wind Energy*, Vol. 12, No. 5, pp. 431-444, 2009

[2] Troen, I., Petersen, E.L., *European Wind Atlas*, Risø National Laboratory, Roskilde, Denmark, 1989:656

[3] Schepers, J.G., *ENDOW: Validation and Improvement of ECN's Wake Model*. ECN:ECN-C-03-034: Petten, The Netherlands, 2003: 113

[4] Crespo, A., Hernandez, J., Fraga, E., Andreu, C., "Experimental validation of the UPM computer code to calculate wind turbine wakes and comparison with other models", *Journal of Wind Engineering and Industrial Aerodynamics*, 1988, 27, pp. 77-88.

[5] Rados, K., Larsen, G., Barthelmie, R., Schelz, W., Lange, B., Schepers, G., Hegberg, T., Magnusson, M., "Comparison of wake models with data for offshore windfarms", *Wind Engineering*, 2002, 25, pp. 271-280

[6] Chaviaropoulos, P.K. and Douvikas, D.I., "Mean-flow-field Simulations over Complex Terrain Using a 3D Reynolds Averaged Navier–Stokes Solver," *Proceedings of ECCOMAS '98*, 1998, Vol. I, Part II, pp. 842-848

[7] Dekker, J.W.M, Pierik, J.T.G. (Editors), "European Wind Turbine Standards II", ECN-C--99-073, 1999

[8] Prospathopoulos, J.M., Politis, E.S., Rados, K.G., Chaviaropoulos, P.K., "Evaluation of the effects of turbulence model enhancements on wind turbine wake predictions", Wind Energy, 2011, 14, pp.285-300.

[9] Politis, E.S., Prospathopoulos, J.M., Cabezon, D., Hansen, K.S., Chaviaropoulos, P.K, Barthelmie,R.J., "Modeling wake effects in large wind farms in complex terrain: the problem, the methods and the issues", Wind Energy, 2012, 15, pp.161-182

[10] Prospathopoulos, J.M., Politis, E.S., Chaviaropoulos, P.K., "Modelling Wind Turbine Wakes in Complex Terrain", *Proceedings of EWEC 2008*, Brussells, Belgium, pp. 42-46

[11] Stull, R. B., "An introduction to boundary layer meteorology", ISBN 90-277-2768-6 ed. Kluwer Publications Ltd, 1988

[12] Panofsky H.A., Dutton J.A., Atmospheric Turbulence, Models and Methods for Engineering Applications, John Wiley & Sons, 1984

[13] Wilcox, D.C., (1993), Turbulence Modelling for CFD, DCW Industries Inc., La Canada, California, IBSN 0-9636051-0-0

[14] Hansen, K. "WP1.1 Wake model performance validations for Horns Rev offshore wind farm" Report: Eera-Dtoc, 2013.

[15] Hansen, K. "WP1.1 Wake model performance validations for Lillgrund offshore wind farm" Report: Eera-Dtoc, 2013.